

Anomalous Collisions of Elastic Vector Solitons in Mechanical Metamaterials

Bolei Deng,¹ Vincent Tournat,^{1,2} Pai Wang,^{1,3} and Katia Bertoldi^{1,4,*}

¹*Harvard John A. Paulson School of Engineering and Applied Sciences, Harvard University, Cambridge, Massachusetts 02138, USA*

²*LAUM, CNRS, Le Mans Université, Avenue Olivier Messiaen, 72085 Le Mans, France*

³*The Concord Consortium, Concord, Massachusetts 01742, USA*

⁴*Kavli Institute, Harvard University, Cambridge, Massachusetts 02138, USA*



(Received 1 November 2018; published 1 February 2019)

We investigate via a combination of experiments and numerical analyses the collision of elastic vector solitons in a chain of rigid units connected by flexible hinges. Because of the vectorial nature of these solitons, very unusual behaviors are observed: while, as expected, the solitons emerge unaltered from the collision if they excite rotations of the same direction, they do not penetrate each other and instead repel one another if they induce rotations of the opposite direction. Our analysis reveals that such anomalous collisions are a consequence of the large-amplitude characteristics of the solitons, which locally modify the properties of the underlying media. Specifically, their large rotations create a significant barrier for pulses that excite rotations of the opposite direction and this may block their propagation. Our findings provide new insights into the collision dynamics of elastic solitary waves. Furthermore, the observed anomalous collisions pave new ways towards the advanced control of large amplitude mechanical pulses, as they provide opportunities to remotely detect, change, or destruct high-amplitude signals and impacts.

DOI: 10.1103/PhysRevLett.122.044101

Collisions are one of the most fascinating features of solitary waves and have been investigated in many areas of science, including optics [1,2], electronics [3], plasmonics [4], quantum mechanics [5], general relativity [6], and mechanics [7–11]. Typically, the solitons are found to emerge from the collision unchanged (except for a phase shift [3–5] or the formation of small secondary waves [7,9,10]), as if there had been no interaction at all. This remarkable behavior led Zabusky and Kruskal [12] to coin the name “soliton” (after photon, proton, etc.), to emphasize the particlelike character of these wave pulses [13–15]. While passing through one another without change of shape, amplitude, or speed is one of the defining properties of solitons [5], few exceptions have been found for solitary waves that propagate in systems that are either damped or not fully integrable. Specifically, the collision between a kink and its antikink pair has been shown to lead to a trapped breather in the integrable sine-Gordon system with damping [16], to a localized bound pair in the nonintegrable ϕ^4 model [17] and to different types of kinks in the nonintegrable double sine-Gordon model [16].

In this study, we focus on a mechanical metamaterial based on rotating rigid units [18–21] and use a combination of experiments and numerical analyses to study the collisions between two supported elastic vector solitons. Surprisingly, despite the fact that the propagation of a single soliton is accurately captured by the completely integrable modified Korteweg–de Vries equation, not all

solitary waves emerge unaltered from the collisions. If the propagating solitons induce rotations of an opposite direction at a given unit in the system, they repel each other upon collision. We show that this highly unusual behavior is closely related to the vectorial nature of the supported solitons, which in turn leads to the formation of amplitude gaps—ranges in amplitude where elastic soliton propagation is forbidden. The large rotations induced by a soliton create a barrier for pulses with a rotational component of the opposite sign that blocks their propagation. Our study provides new insights into the collision dynamics of elastic solitary waves and reveals that in vector solitons the coupling between the different components can lead to completely unexplored and new phenomena.

Our mechanical metamaterial consists of a chain of N pairs of rigid crosses connected by thin and flexible hinges [see Fig. 1(a)]. It has been recently shown that the propagation of a single soliton in such a system is accurately described by a nonlinear Klein-Gordon equation [19], which can be rewritten in the form of the completely integrable Korteweg–de Vries equation [22]. The solution of such an equation indicates that the considered metamaterial supports the propagation of elastic vector solitons that induce simultaneous longitudinal displacement u_i and rotation θ_i at the i th pair of crosses, with all neighboring units rotating in opposite directions [see Fig. 1(a)]. Specifically, u_i and θ_i are defined by [19] (see Supplemental Material [23])

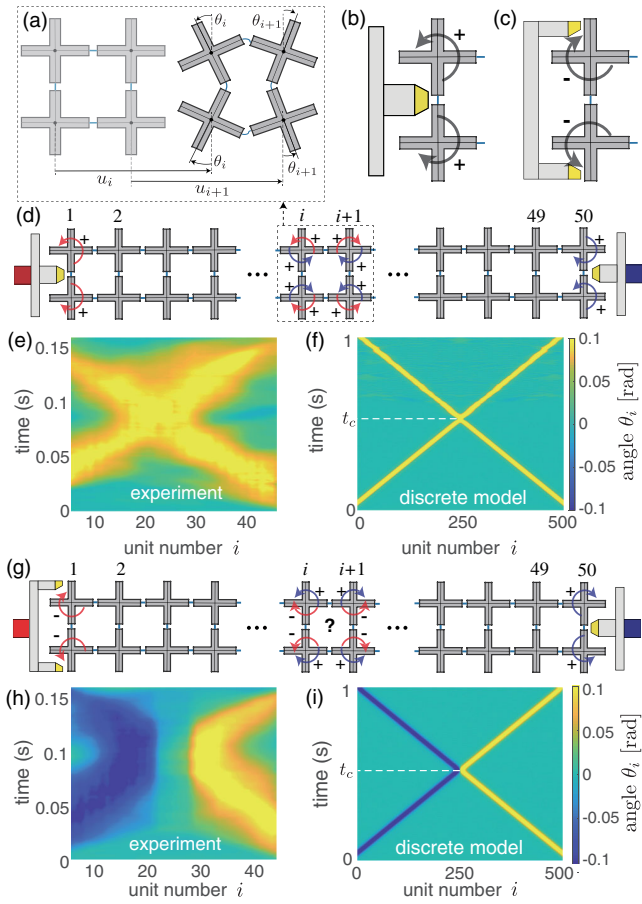


FIG. 1. (a) Schematic of the system. (b),(c) Schematics of the impactors used to excite (b) positive and (c) negative rotations. (d) Schematic of our first experiment. (e),(f) Rotation of the pairs of crosses during the propagation of the pulses, as recorded during our first test in (e) experiments and (f) numerical simulations. (g) Schematic of our second experiment. (h),(i) Rotation of the pairs of crosses during the propagation of the pulses, as recorded during our second test in (h) experiments and (i) numerical simulations.

$$u_i(t) = \frac{aA^2W}{2(1 - c^2/c_0^2)} \left[1 - \tanh\left(\frac{ia - ct}{W}\right) \right], \quad (1)$$

and

$$\theta_i(t) = A \operatorname{sech}\left(\frac{ia - ct}{W}\right), \quad (2)$$

where a denotes the center-to-center distance between neighboring units and c_0 is the velocity of the supported linear longitudinal waves in the long wavelength limit. Moreover, A , c , and W denote the amplitude, speed, and width of the pulses, with speed and width that can be expressed in terms of amplitude as

$$c = \pm c_0 \sqrt{\frac{6K_\theta}{A^2 + 6K_\theta}}, \quad (3)$$

and

$$W = \frac{a}{\alpha} \sqrt{\frac{\alpha^2(K_s - K_\theta) - 6K_\theta/(A^2 + 6K_\theta)}{6K_\theta}}. \quad (4)$$

where α represents the normalized mass, and K_s and K_θ are the normalized shear and bending stiffnesses of the hinges. At this point it is important to note that the propagation of the vector solitons defined by Eqs. (1) and (2) requires a strong coupling among their two components u_i and θ_i [24]. Since in our system such a strong coupling is activated only for large enough rotations, vector solitons with

$$|A| < \sqrt{\frac{6K_s}{\alpha^2(K_s - K_\theta)} - 6K_\theta} \quad (5)$$

cannot propagate, resulting in the emergence of amplitude gaps [19]. While Eq. (5) fully defines the amplitude gap for a chain in which all hinges are aligned, prerotations of the crosses significantly increase the magnitude of the lower threshold, as they make the propagation of solitons that induce energetically unfavorable rotation more difficult [19]. Notably, our analysis will reveal that such a prerotation effect on the amplitude gap plays a central role in defining the collision dynamics.

To investigate the collision of solitons in our system, we test a structure comprising $N = 50$ pairs of crosses made with LEGO bricks and connected via polyester plastic sheets. To initiate elastic vector solitons, we use two impactors that induce simultaneous rotation and displacement of the crosses at both ends of the sample [see Figs. 1(b) and 1(c), and the Supplemental Material [23]]. We control the amplitude of the pulses by varying the maximum distance traveled by the impactors. As for the direction of rotation imposed to the first and last pairs of crosses, we select it by using two different types of impactors. Specifically, since we define as positive a clockwise (counterclockwise) rotation of the top unit in the even (odd) pairs, we use an impactor that hits the midpoint of the end pairs to excite positive θ_i [see Fig. 1(b)] and one that hits their external arms to excite negative θ_i [see Fig. 1(c)]—note that the direction of rotations imposed by the impactors changes if the chain comprises an odd number of pairs, see Supplemental Material [23]]. In addition to the experiments, we also simulate the response of a chain with $N = 500$ pairs of crosses (to eliminate possible boundary effects) by numerically integrating the $2N$ ordinary differential equations with parameters $\alpha = 1.8$, $K_s = 0.02$ and $K_\theta = 1.5 \times 10^{-4}$ [19].

In Figs. 1(e), 1(f), 1(h), and 1(i), we present experimental and numerical results for two sets of input signals applied to the left and right ends of the chain. First, the impactors excite solitons with amplitude $A_{\text{left}} = A_{10} = 0.2$ and $A_{\text{right}} = A_{N-10} = 0.2$ (A_i being the amplitude of θ_i

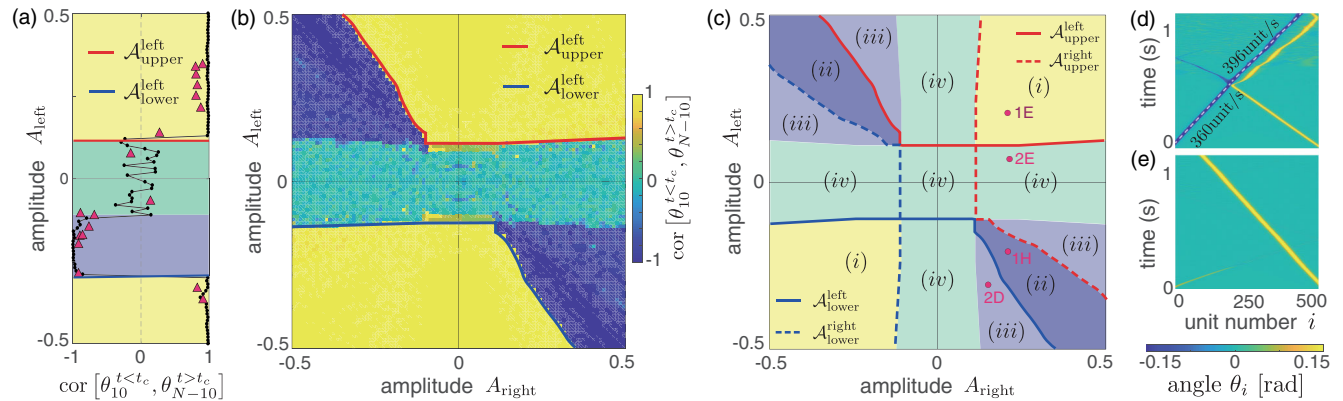


FIG. 2. (a) Cross-correlation between $\theta_{10}(t < t_c)$ and $\theta_{N-10}(t > t_c)$ as a function of A_{left} for $A_{\text{right}} = 0.2$. Triangular markers correspond to experimental data, while the black line is generated using numerical simulations. (b) Numerically obtained cross-correlation between $\theta_{10}(t < t_c)$ and $\theta_{N-10}(t > t_c)$ as a function of A_{left} and A_{right} . (c) Complete picture of the collision dynamic between the pulses supported by the system. (d),(e) Rotations of the pairs of crosses during the propagation of the pulses as found in numerical simulations for (d) $(A_{\text{left}}, A_{\text{right}}) = (-0.3, 0.22)$ and (e) $(0.08, 0.3)$.

before the collision). Both our experimental and numerical results indicate that the two pulses, which induce rotations with the same direction at any given unit in the chain [see Fig. 1(d)], penetrate each other without change of shape, amplitude, or speed [see Figs. 1(e) and 1(f) and Movie 1 in the Supplemental Material [23]]. As commonly observed when two solitons collide [3,4,4–7,9,10], only a slight time delay may be observed, confirming that our metamaterial can respond similarly to a fully integrable system such as a KdV system [16,25]. Second, we apply $A_{\text{left}} = -0.2$ and $A_{\text{right}} = 0.2$ to excite two pulses that induce rotations of an opposite sign at any given unit [see Fig. 1(g)]. Surprisingly, we find that in this case the solitons do not penetrate each other and instead reflect one another [see Figs. 1(h) and 1(i) and Movie 1 in the Supplemental Material [23]]. This phenomenon is especially visible from the absence of rotations of the units in the center of the system. It is also important to note that, while in the experiments there is inevitably some dissipation due to both friction and viscous effects, in our numerical simulation we do not include any damping. As such, our results indicate that the observed anomalous collisions are not due to the presence of damping or boundary effects, and are rather a robust feature of the system.

To better understand how two colliding solitons interact in our system, we focus on the left-initiated pulse and systematically investigate how it is affected by the collision with the right-initiated one. To quantify such an effect, we calculate the cross-correlation between $\theta_{10}(t < t_c)$ and $\theta_{N-10}(t > t_c)$ (t_c denoting the time at which the collision occurs) as a function of A_{left} , while keeping $A_{\text{right}} = 0.2$. As shown in Fig. 2(a), we find that the response of the system is characterized by two distinct regions. For $A_{\text{left}} < A_{\text{lower}}^{\text{left}} = -0.28$ and $A_{\text{left}} > A_{\text{upper}}^{\text{left}} = 0.12$ the left-initiated elastic vector solitons propagate through the entire structure

unaffected by the collision with the right-initiated pulses and the cross-correlation approaches unity. By contrast, for $A_{\text{lower}}^{\text{left}} < A_{\text{left}} < A_{\text{upper}}^{\text{left}}$ the left-initiated pulse does not reach the other end of the chain and the cross-correlation is $\ll 1$. Focusing on this region of low cross-correlation, two recognizably different behaviors are observed. First, for $-0.12 < A_{\text{left}} < A_{\text{upper}}^{\text{left}}$ the cross-correlation approaches zero, since the propagation of the left-initiated soliton is prevented by the amplitude gap of the chain defined by Eq. (5) (note that for this range of amplitudes no collision occurs, since the left-initiated soliton dies before reaching the right-initiated one). Second, for $A_{\text{lower}}^{\text{left}} < A_{\text{left}} < -0.12$ the cross-correlation approaches -1 . For this range of amplitudes a solitary wave that induces rotations with a direction opposite from those excited by the left-initiated soliton is detected at the right end after collision—a clear signature of an anomalous collision dynamics that results in the (partial or total) reflection of the right-initiated soliton.

Next, we consider the effect on the collision of both A_{left} and A_{right} . The heat map shown in Fig. 2(b) confirms that, while typical collisions that do not alter the left-initiated soliton (resulting in a cross-correlation that approaches 1) occur when the two colliding solitons induce rotation of the same direction (i.e., $A_{\text{left}}A_{\text{right}} > 0$), anomalous collisions that change the left-initiated pulse (leading to a cross-correlation $\ll 1$) may also exist when two colliding solitons induce rotations of the opposite direction (i.e., $A_{\text{left}}A_{\text{right}} < 0$). We then construct a plot analogous to that shown in Fig. 2(b), but focused on the right-initiated pulses by considering the cross-correlation between $\theta_{N-10}(t < t_c)$ and $\theta_{10}(t > t_c)$ (see Fig. S7). By combining Fig. 2(b) with Fig. S7, we find that four different scenarios are possible upon collision [see Fig. 2(c)]: (i) both solitons penetrate, as typical for collisions between solitons [see yellow area in Fig. 2(c) and Figs. 1(d) and 1(e)]; (ii) both solitons are reflected—a clear signature of an anomalous collision (see

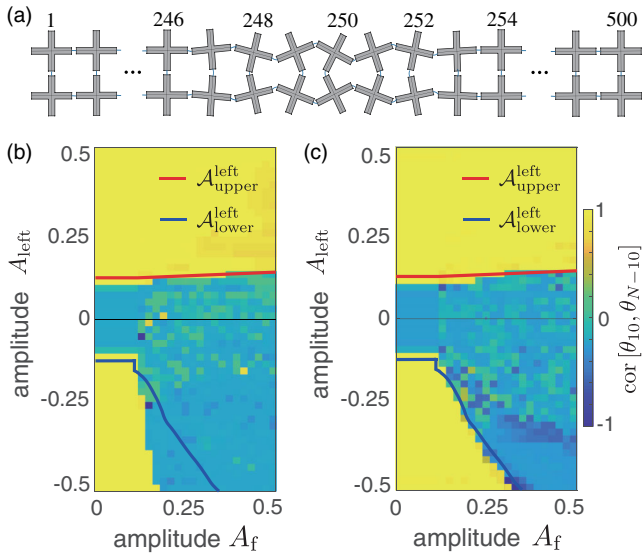


FIG. 3. (a) A $N = 500$ chain with a frozen soliton placed in the middle of it. (b),(c) Numerically obtained cross-correlation between $\theta_{10}(t)$ and $\theta_{N-10}(t)$ as a function of A_{left} and A_f with frozen solitons of width defined by (b) W_f and (c) W_f^{eff} .

dark blue area in Figs. 2(c), 1(g), and 1(h); (iii) one soliton is blocked and the other penetrates—again the signature of an anomalous collision [see shallow blue area in Figs. 2(c) and 2(d)]; (iv) one or no soliton travels through the system due to the existence of the amplitude gap, so that no collision occurs [see green area in Figs. 2(c) and 2(e)]. Therefore, our numerical investigation describes quantitatively all possible two-soliton heads-on collisions and provides a complete picture of the collision dynamic between the pulses supported by the system.

The results of Figs. 1 and 2 reveal that our system supports anomalous collisions that alter the characteristics of the solitons. Such a surprising phenomenon can be fully explained via the concept of amplitude gaps. The large rotations generated by a soliton effectively enlarge the amplitude gap for pulses that induce rotations of the opposite sign, stopping their propagation when they come close enough. To demonstrate this important point, we freeze solitons of different amplitude A_f in the middle of the chain and numerically investigate their effect on the propagation of solitary waves initiated at the left end. Specifically, we consider a chain in which the i th pair of crosses is rotated according to theoretical solution of soliton [see Fig. 3(a) and the Supplemental Material [23]], excite pulses of different amplitude A_{left} at its left end, and investigate the interaction between the left-initiated soliton and the frozen perturbation by looking at the cross-correlation between $\theta_{10}(t)$ and $\theta_{N-10}(t)$. The numerical results reported in Fig. 3(b) clearly indicate that there is a well-defined region in the $A_{\text{left}} - A_f$ space resulting in left-initiated solitons that do not reach the right end of the chain (note that in this region the cross-correlation is close to zero

everywhere, as there is no propagating right-initiated pulse that can be reflected). Notably, we also find that the lower thresholds of the low cross-correlation region obtained considering a frozen perturbation or a right-initiated pulse follow similar trends [see Fig. 3(b)]. However, there is a significant quantitative discrepancy between them that arises because the left-initiated soliton interacts for a time $\Delta t \propto (c_{\text{left}} + c_{\text{right}})^{-1}$ with the right-initiated pulse (c_{left} and c_{right} denoting the velocities of the left-initiated and right-initiated solitary waves before collision, respectively) and $\Delta t \propto c_{\text{left}}^{-1}$ with the frozen perturbation. To overcome this difference, we equate the interaction times by shrinking the width of the frozen soliton according to

$$W_f^{\text{eff}} = \frac{c_{\text{left}}}{c_{\text{right}} + c_{\text{left}}} W_f, \quad (6)$$

where c_{right} is given by Eq. (3) with $A = A_f$. Remarkably, by replacing the width of the frozen solitons W_f with W_f^{eff} , we find that the boundaries of the low cross-correlation region match extremely well the thresholds $\mathcal{A}_{\text{upper}}^{\text{left}}$ and $\mathcal{A}_{\text{lower}}^{\text{left}}$ [see Fig. 3(c)]. As such, our analysis reveals that the anomalous collisions observed in our system are a consequence of the soliton large-amplitude characteristics, which modify the properties of the underlying media. Specifically, the large rotations induced in the chain by a pulse enlarge the amplitude gap for solitons that excite rotations of the opposite direction and this may block their propagation.

While in Figs. 1–3 we focus on the interaction between pulses initiated at the two ends of the chain, anomalous collisions can also be triggered when the solitons are sequentially excited at the same end. To demonstrate this, we numerically study the collision between two solitons with amplitude $A_{\text{left},1}$ and $A_{\text{left},2}$ initiated at the left end at time $t_1 = 0$ and $t_2 = 0.3$ s, respectively. We find that if the two solitons excite rotations of the same sign and the second one is faster, the second pulse penetrates and overtakes the first one, and neither of them change their amplitude, shape, or velocity [see Fig. 4(a)]. By contrast, if the two solitons induce rotations of the opposite sign, a single pulse emerges from the collision with the same direction as the first one, but with a larger amplitude and, therefore, lower velocity [see Fig. 4(b)].

Having demonstrated that our system can support anomalous collisions that alter the characteristics of the interacting solitons, we now explore how these unusual effects can be exploited to actively manipulate and control the propagation of pulses. First, we note that anomalous collisions provide opportunities to remotely induce changes in the propagation velocity of a soliton, as they can either reverse [see Figs. 1(h) and 1(i)], increase [see Fig. 2(d)] or lower [see Fig. 4(b)] the pulses speed (see also Fig. S8A in the Supplemental Material [23]). Second, we find that anomalous collisions can be exploited to probe the direction of the rotations of a pulse by monitoring the “echo” of

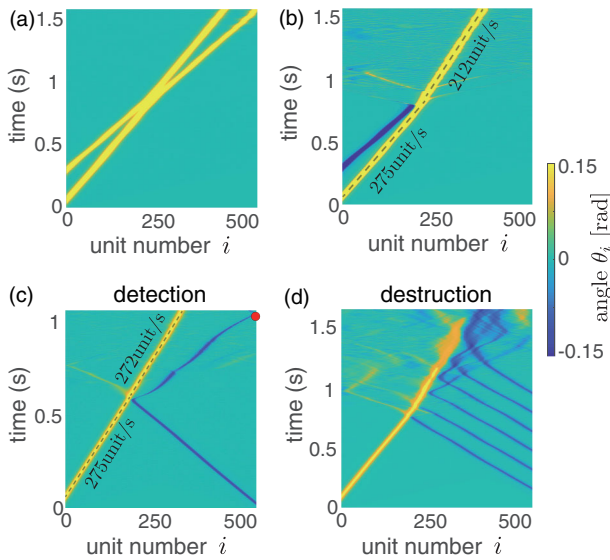


FIG. 4. (a),(b) Rotations of the pairs of crosses as numerically found when considering two solitons of amplitude $A_{\text{left},1}$ and $A_{\text{left},2}$ initiated at the left end at time $t_1 = 0$ and $t_2 = 0.3$ s. ($A_{\text{left},1}, A_{\text{left},2}$) = (0.4, 0.3) in (a) and (0.4, -0.3) in (b). (c) A soliton with amplitude $A_{\text{right}} = -0.18$ is excited from the right end as a probing soliton to detect the rotation direction of the main soliton of amplitude $A_{\text{left}} = 0.4$. (d) An amplitude $A_{\text{left}} = 0.4$ soliton is destroyed by six small solitons of amplitude $A_{\text{right},k} = -0.2$ (with $k = 1, \dots, 6$).

a probing soliton [see Fig. 4(c) and Supplemental Material [23], Fig. S8]. Third, if the direction of rotations excited by the soliton is known, we can block its propagation by sending a sequence of relatively small pulses with an opposite rotation direction (see Figs. 4(d) and S8).

To summarize, our experiments show that anomalous interactions can occur for vector elastic solitons supported by a mechanical metamaterial based on rigid rotating units. While two solitons that induce rotations of the same direction penetrate each other when they meet, two solitons with an opposite rotational component may repel each other and change both their amplitudes and velocities upon collision. Remarkably, our numerical analyses can fully explain the experimental findings and provide a complete description of these exotic two-soliton interactions. The geometric changes induced by one soliton significantly enlarge the effective amplitude gaps for other solitons with an opposite rotational component and may block their propagation when they come close enough. We envision that the reported anomalous collisions between solitons could be used for remote control of the propagating nonlinear pulses, as they result in changes of the pulse velocity that can be engineered to remotely detect, change, or destruct high-impact signals.

K. B. acknowledges support from the National Science Foundation under Grant No. DMR-1420570 and

No. EFMA-1741685 and from the Army Research Office under Grant No. W911NF-17-1-0147.

*bertoldi@seas.harvard.edu

- [1] G. I. Stegeman and M. Segev, *Science* **286**, 1518 (1999).
- [2] R. Radhakrishnan, M. Lakshmanan, and J. Hietarinta, *Phys. Rev. E* **56**, 2213 (1997).
- [3] T. Tsuboi, *Phys. Rev. A* **40**, 2753 (1989).
- [4] H. K. Malik, R. Kumar, K. E. Lonngren, and Y. Nishida, *Phys. Rev. E* **92**, 063107 (2015).
- [5] J. H. V. Nguyen, P. Dyke, D. Luo, B. A. Malomed, and R. G. Hulet, *Nat. Phys.* **10**, 918 (2014).
- [6] J. Ibañez and E. Verdaguer, *Phys. Rev. Lett.* **51**, 1313 (1983).
- [7] S. Sen, J. Hong, J. Bang, E. Avalos, and R. Doney, *Phys. Rep.* **462**, 21 (2008).
- [8] H. Yasuda, Y. Miyazawa, E. G. Charalampidis, C. Chong, P. G. Kevrekidis, and J. Yang, [arXiv:1805.05909](https://arxiv.org/abs/1805.05909).
- [9] F. Santibanez, R. Munoz, A. Caussarie, S. Job, and F. Melo, *Phys. Rev. E* **84**, 026604 (2011).
- [10] M. Manciu, S. Sen, and A. J. Hurd, *Phys. Rev. E* **63**, 016614 (2000).
- [11] P. Anzel and C. Daraio, *Proc. SPIE* **8346**, 1 (2012).
- [12] N. J. Zabusky and M. D. Kruskal, *Phys. Rev. Lett.* **15**, 240 (1965).
- [13] M. I. Hussein, M. J. Leamy, and M. Ruzzene, *Appl. Mech. Rev.* **66**, 040802 (2014).
- [14] P. Drazin and R. Johnson, *Solitons: An Introduction*, Cambridge Texts in Applied Mathematics (Cambridge University Press, Cambridge, England, 1989).
- [15] G. Theocharis, N. Boechler, and C. Daraio, Nonlinear periodic phononic structures and granular crystals, *Acoustic Metamaterials and Phononic Crystals*, edited by P. Deymier, in Springer Series in Solid-State Sciences Vol. 173 (Springer, Berlin, Heidelberg, 2013).
- [16] T. Dauxois and M. Peyrard, *Physics of Solitons* (Cambridge University Press, Cambridge, England, 2006).
- [17] V. G. Makhankov, *Soliton Phenomenology* (Kluwer Academic, Dordrecht, 1989).
- [18] B. Deng, J. R. Raney, V. Tournat, and K. Bertoldi, *Phys. Rev. Lett.* **118**, 204102 (2017).
- [19] B. Deng, P. Wang, Q. He, V. Tournat, and K. Bertoldi, *Nat. Commun.* **9**, 3410 (2018).
- [20] B. Deng, V. Tournat, and K. Bertoldi, *Phys. Rev. E* **98**, 053001 (2018).
- [21] C. Coulais, C. Kettenis, and M. van Hecke, *Nat. Phys.* **14**, 40 (2018).
- [22] A. Polyanin and V. Zaitsev, *Handbook of Nonlinear Partial Differential Equations* (Chapman and Hall/CRC, Boca Raton, Florida, 2011).
- [23] See Supplemental Material at <http://link.aps.org/supplemental/10.1103/PhysRevLett.122.044101> for additional fabrication, experimental, numerical and theoretical details.
- [24] Y. S. Kivshar, *J. Opt. Soc. Am. B* **7**, 2204 (1990).
- [25] M. Tabor, *Chaos and Integrability in Nonlinear Dynamics* (Wiley, Hoboken, New Jersey, 1989).

Supporting Information for

Anomalous collisions of elastic vector solitons in mechanical metamaterials

Bolei Deng¹, Vincent Tournat^{1,2}, Pai Wang¹, Katia Bertoldi^{1, 3*}

¹Harvard John A. Paulson School of Engineering and Applied Sciences
Harvard University, Cambridge, Massachusetts 02138, USA

²LAUM UMR CNRS, Le Mans Université, 72085 Le Mans, France

³ Kavli Institute, Harvard University, Cambridge, Massachusetts 02138, USA

*To whom correspondence should be addressed; E-mail: bertoldi@seas.harvard.edu

November 7, 2018

S1 Fabrication

Our system is identical to that recently considered in (1) and consists of a long chain of 2×50 crosses made of LEGO bricks that are connected by thin and flexible hinges made of plastic shims. Each cross-shaped unit is realized using four brackets $2 \times 2-2 \times 2$ (LEGO part 3956), as shown in Fig. S1. The hinges are realized by laser cutting the octagonal shape shown in Fig. S1A out of polyester plastic sheets (Artus Corporation, NJ - 0.005", Blue) with thickness $t_h = 0.127$ mm, Young's modulus $E = 4.33$ GPa and Poisson's ratio $\nu = 0.4$. The size of the octagonal shape is chosen to leave hinges of length $l_h = 4$ mm between the cross-shaped rigid units. Note that eight circular holes are incorporated into each hinge. They fit into the LEGO knobs and enable us to fix the hinges between the interlocking LEGO bricks (see

Fig. S1B). Note that in both samples identical bricks of different colors (black and gray) are used to facilitate visualization of the propagating pulses.

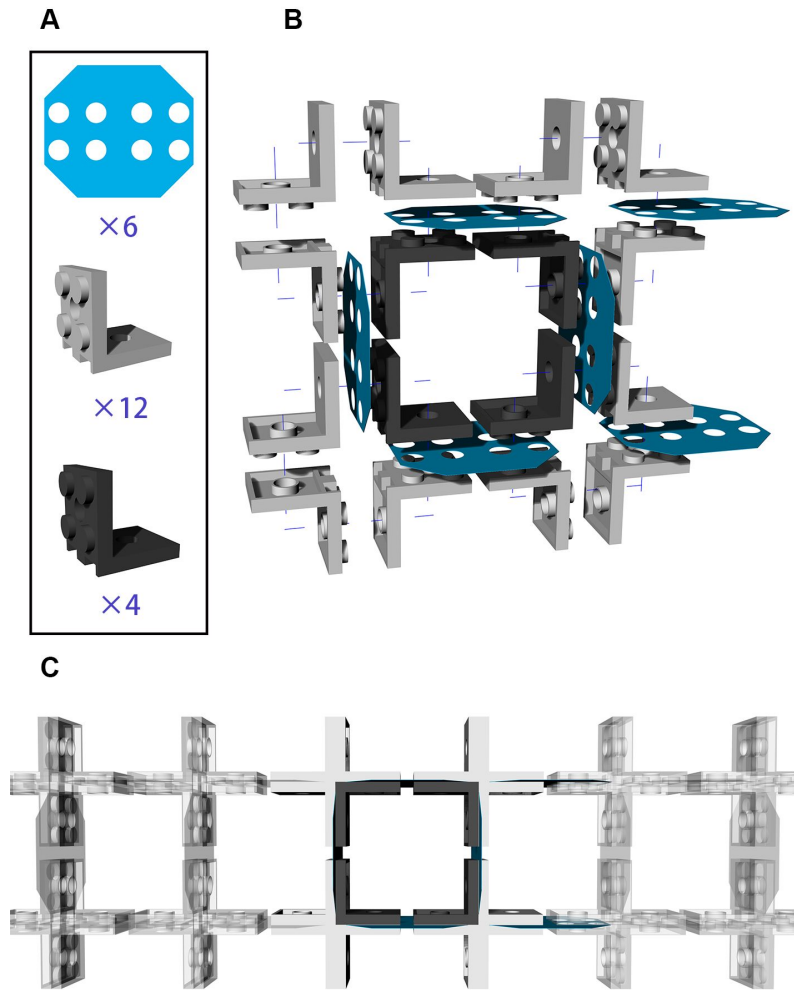


Figure S1: Fabrication of our structure. (A) Parts used to fabricate a 2×2 unit. (B) Exploded view of two pairs of crosses. (C) The chain is realized by putting together a number of 2×2 units.

S2 Testing

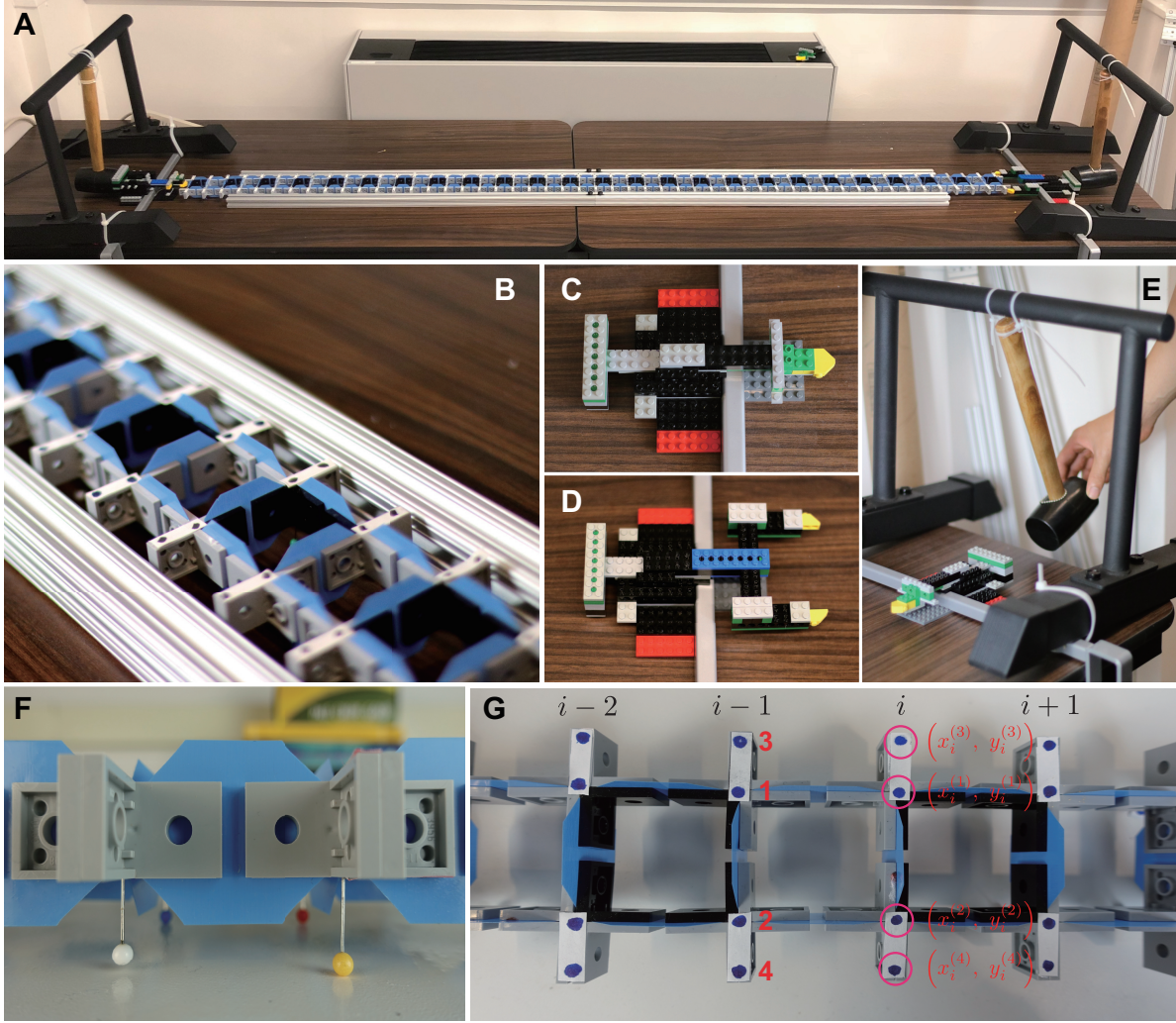


Figure S2: Experimental setup. (A) Pictures of our experimental setup showing the LEGO chain, the metal bars used to constrain the transverse movement of the chain and the pendulums and impactors used to excite the pulses at both ends. (B) A few units of our sample. (C) The impactor used to initiate solitons that excite positive rotations. (D) The impactor used to initiate solitons that excite negative rotations. (E) Close view of the pendulum consisting of a metal frame and a hammer. (F) Friction is minimized by supporting each rigid unit with pins. (G) Digital image correlation analysis. For each pair of rigid crosses four markers (blue dots) are tracked.

To investigate the propagation of pulses in our sample, we place the chain on a smooth horizontal surface (supported by pins to minimize the effect of friction - see S2F) and use two impactors excited by two pendulums (see Fig. S2A-B) to initiate the waves. Two metal bars are

placed on both sides of the chain to keep it straight. Note that the metal bars are not interacting with the chain during the propagation of nonlinear waves since the structure shrinks transversely due to the rotation of crosses. Different input signals are applied to the chain by varying both the strength of the pulse (controlled by the initial height of the striking pendulum) and the amplitude of the pulse (controlled by the distance traveled by the impactor). Furthermore, the direction of rotation imposed to the first and last pairs of crosses is controlled by using two different types of impactors. Specifically, since we define as positive a clockwise (counter-clockwise) rotation of the top unit in the even (odd) pairs, we use an impactor that hits the mid-point of the end pairs to excite positive rotation (see Fig. S2C) and one that hit their external arms to excite negative θ_i (see Fig. S2D). At this point we also want to point out that the direction of rotations imposed by the impactors changes if the chain comprises an odd number of pairs. If the chain has a odd number of pairs, the impactor that hits the mid-point of the last pair excite negative rotations (see Fig. S2C) and the one that hit the external arms of the last pair excite negative rotations (see Fig. S2D).

To monitor the displacement, u_i , and rotation, θ_i , of i -th pair of crosses along the chain as the pulses propagate, we use a high speed camera (SONY RX100V) recording at 480 fps and track four markers placed on the external arms of each pair of crosses (see S2G) via digital image correlation analysis (2). More specifically, the longitudinal displacement u_i and rotation θ_i of the i -th pair of rigid units is obtained as

$$u_i(t) = \frac{1}{2} \sum_{\gamma=1,2} \left[x_i^{(\gamma)}(t) - x_i^{(\gamma)}(0) \right]$$

$$\theta_i(t) = \frac{1}{2} \sum_{\gamma=1,2} (-1)^{i+\gamma} \arcsin \left[\frac{\left(x_i^{(\gamma+2)}(t) - x_i^{(\gamma+2)}(0) \right) - \left(x_i^{(\gamma)}(t) - x_i^{(\gamma)}(0) \right)}{\sqrt{\left(x_i^{(\gamma+2)}(0) - x_i^{(\gamma)}(0) \right)^2 + \left(y_i^{(\gamma+2)}(0) - y_i^{(\gamma)}(0) \right)^2}} \right] \quad (\text{S1})$$

where $(x_i^{(\gamma)}(t), y_i^{(\gamma)}(t))$ and $(x_i^{(\gamma)}(0), y_i^{(\gamma)}(0))$ are the coordinates of the γ -th marker placed on the i -th pair of rigid units at time t and that time $t = 0$ (i.e. before the impact), respectively.

S3 Mathematical Models

S3.1 Discrete model

Our system consists of a long chain of $2 \times N$ crosses with center-to-center distance a that are connected by thin and flexible hinges (see Fig. S3). Since in this work we focus on the propagation of longitudinal nonlinear waves along the chain, we assign two degrees of freedom to each rigid cross: the longitudinal displacement u and the rotation in the $x - y$ plane θ . Moreover, guided by our experiments, we assume that each pair of crosses shares the same displacement and rotates by the same amount, but in opposite directions (i.e. if the top cross rotates by a certain amount in clockwise direction, then the bottom one rotates by the same amount in counter-clockwise direction, and vice versa). As such, two degrees of freedom are assigned to the i -th pair of crosses: the longitudinal displacement u_i and the rotation θ_i (see Fig. S3).

Moreover, to facilitate the analysis, we define a clockwise (counter-clockwise) rotation of the

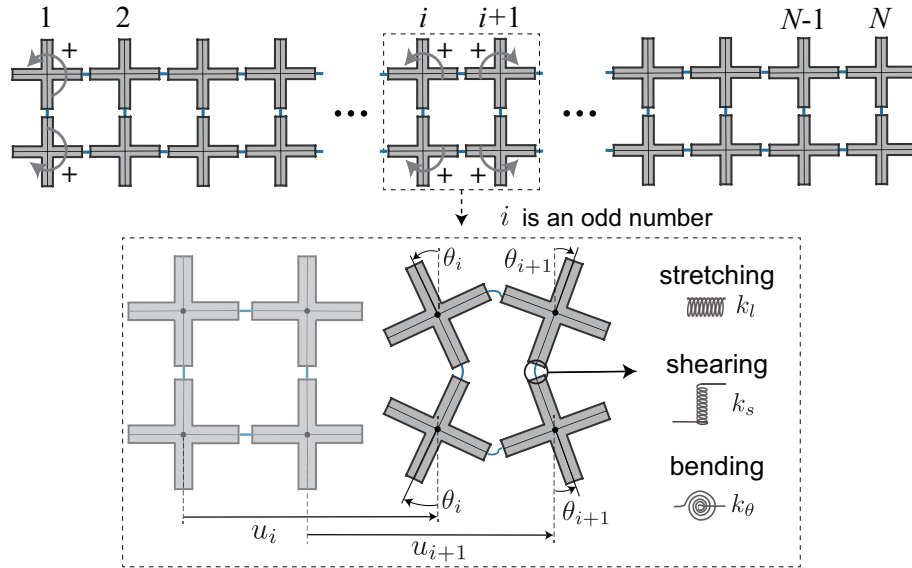


Figure S3: Schematics of the structure considered in this study.

top unit in the even (odd) columns to be positive, and similarly a clockwise (counter-clockwise) rotation of the bottom unit in the odd (even) columns to be negative (positive rotation directions

are denoted by yellow arrows in Fig. S3).

As for the hinges, we model them using a combination of three linear springs: (i) their stretching is captured by a spring with stiffness k_l ; (ii) their shearing is governed by a spring with stiffness k_s ; (iii) their bending is captured by a torsional spring with stiffness k_θ (see Fig. S3).

Under these assumptions, the equations of motion for the i -th pair of crosses are given by (1)

$$\begin{aligned} m\ddot{u}_i &= k_l \left[u_{i+1} - 2u_i + u_{i-1} - \frac{a}{2} (\cos \theta_{i+1} - \cos \theta_{i-1}) \right], \\ J\ddot{\theta}_i &= -k_\theta(\theta_{i+1} + 4\theta_i + \theta_{i-1}) + \frac{k_s a^2}{4} \cos \theta_i [\sin \theta_{i+1} - 2 \sin \theta_i + \sin \theta_{i-1}] \\ &\quad - \frac{k_l a}{2} \sin \theta_i \left[(u_{i+1} - u_{i-1}) + \frac{a}{2} (4 - \cos \theta_{i+1} - 2 \cos \theta_i - \cos \theta_{i-1}) \right], \end{aligned} \quad (\text{S2})$$

where m and J are the mass and moment of inertia of the rigid crosses, respectively.

Next, we introduce the normalized inertia $\alpha = a\sqrt{m/(4J)}$ and stiffness ratios $K_\theta = 4k_\theta/(k_l a^2)$ and $K_s = k_s/k_l$. Eqs. (S2) can then be written in dimensionless form as

$$\begin{aligned} \frac{a^2}{c_0^2} \frac{\partial^2 u_i}{\partial t^2} &= u_{i+1} - 2u_i + u_{i-1} - \frac{a}{2} [\cos \theta_{i+1} + \cos \theta_{i-1}], \\ \frac{a^2}{c_0^2 \alpha^2} \frac{\partial^2 \theta_i}{\partial t^2} &= -K_\theta(\theta_{i+1} + 4\theta_i + \theta_{i-1}) + K_s \cos \theta_i [\sin \theta_{i+1} + \sin \theta_{i-1} - 2 \sin \theta_i] \\ &\quad - \sin \theta_i [2(u_{i+1} - u_{i-1})/a + 4 - \cos \theta_{i+1} - 2 \cos \theta_i - \cos \theta_{i-1}], \end{aligned} \quad (\text{S3})$$

where $c_0 = a\sqrt{k_l/m}$ is the velocity of the longitudinal linear waves supported by the chain in the long wavelength limit. As described in section S4, since it is extremely challenging to derive an analytical solution that captures the interaction between the solitons propagating in our system, we study collisions by numerically integrating the $2N$ coupled ordinary differential equations given by Eqs. (S3). Finally, we note that for the system considered in this study $K_s = 0.02$, $K_\theta = 1.5 \times 10^{-4}$ and $\alpha = 1.8$ (I).

S3.2 Analytical solution for a single pulse

Although it is extremely challenging to analytically describe the interactions between the pulses supported by our system, here we derive an analytical model to better characterize the propagation of a single wave. To this end, as recently shown in (1), we introduce two continuous functions $u(x, t)$ and $\theta(x, t)$ that interpolate the displacement and rotation of the i -th pair of crosses located at $x_i = ia$ as

$$u(x_i, t) = u_i(t), \quad \theta(x_i, t) = \theta_i(t). \quad (\text{S4})$$

Assuming that the width of the propagating waves is much larger than the unit cell size, the displacement u and rotation θ in correspondence of the $i+1$ and $i-1$ -th pairs of crosses can then be expressed using Taylor expansion as

$$\begin{aligned} u_{i\pm 1}(t) &= u(x_{i\pm 1}, t) \approx u\Big|_{x_i, t} \pm a\frac{\partial u}{\partial x}\Big|_{x_i, t} + \frac{a^2}{2}\frac{\partial^2 u}{\partial x^2}\Big|_{x_i, t} \\ \theta_{i\pm 1}(t) &= \theta(x_{i\pm 1}, t) \approx \theta\Big|_{x_i, t} \pm a\frac{\partial \theta}{\partial x}\Big|_{x_i, t} + \frac{a^2}{2}\frac{\partial^2 \theta}{\partial x^2}\Big|_{x_i, t} \\ \cos \theta_{i\pm 1}(t) &= \cos [\theta(x_{i\pm 1}, t)] \approx \cos \theta\Big|_{x_i, t} \pm a\frac{\partial \cos \theta}{\partial x}\Big|_{x_i, t} + \frac{a^2}{2}\frac{\partial^2 \cos \theta}{\partial x^2}\Big|_{x_i, t} \\ \sin \theta_{i\pm 1}(t) &= \sin [\theta(x_{i\pm 1}, t)] \approx \sin \theta\Big|_{x_i, t} \pm a\frac{\partial \sin \theta}{\partial x}\Big|_{x_i, t} + \frac{a^2}{2}\frac{\partial^2 \sin \theta}{\partial x^2}\Big|_{x_i, t} \end{aligned} \quad (\text{S5})$$

Substitution of Eqs. (S5) into Eqs. (S3) yields

$$\begin{aligned} \frac{1}{c_0^2} \frac{\partial^2 u}{\partial t^2} &= \frac{\partial^2 u}{\partial x^2} - \frac{\partial \cos \theta}{\partial x}, \\ \frac{a^2}{c_0^2 \alpha^2} \frac{\partial^2 \theta}{\partial t^2} &= -a^2 K_\theta \frac{\partial^2 \theta}{\partial x^2} + a^2 K_s \cos \theta \frac{\partial^2 \sin \theta}{\partial x^2} + a^2 \sin \theta \frac{\partial^2 \cos \theta}{\partial x^2} \\ &\quad - 6K_\theta \theta - 4 \sin(\theta) \left[\frac{\partial u}{\partial x} + 1 - \cos \theta \right], \end{aligned} \quad (\text{S6})$$

which represent the continuum governing equations of the system. Since these two coupled partial differential equations cannot be solved analytically, guided by our experiments, we further

assume that $\theta \ll 1$, so that

$$\sin \theta \approx \theta - \frac{\theta^3}{6}, \text{ and } \cos \theta \approx 1 - \frac{\theta^2}{2}. \quad (\text{S7})$$

By substituting Eqs. (S7) into Eqs. (S6) and retaining the nonlinear terms up to third order, we obtain

$$\begin{aligned} \frac{1}{c_0^2} \frac{\partial^2 u}{\partial t^2} &= \frac{\partial^2 u}{\partial x^2} + \theta \frac{\partial \theta}{\partial x}, \\ \frac{a^2}{c_0^2 \alpha^2} \frac{\partial^2 \theta}{\partial t^2} &= a^2 (K_s - K_\theta) \frac{\partial^2 \theta}{\partial x^2} - 4 \left[\frac{3K_\theta}{2} + \frac{\partial u}{\partial x} \right] \theta - 2\theta^3, \end{aligned} \quad (\text{S8})$$

Finally, we introduce the traveling wave coordinate $\zeta = x - ct$, c being the pulse velocity, so that Eqs. (S8) become

$$\begin{aligned} \frac{\partial^2 u}{\partial \zeta^2} &= -\frac{1}{1 - c^2/c_0^2} \theta \frac{\partial \theta}{\partial \zeta} \\ \beta^{-1} \frac{\partial^2 \theta}{\partial \zeta^2} &= 4 \left[\frac{3K_\theta}{2} + \frac{\partial u}{\partial x} \right] \theta + 2\theta^3, \end{aligned} \quad (\text{S9})$$

where

$$\beta = a^{-2} \left[K_s - K_\theta - \frac{c^2}{\alpha^2 c_0^2} \right]^{-1} \quad (\text{S10})$$

By integrating Eq. (S9)₁ with respect to ζ we obtain,

$$\frac{\partial u}{\partial \zeta} = -\frac{1}{1 - c^2/c_0^2} \frac{\theta^2}{2} + C \quad (\text{S11})$$

where C is the integration constant. Since in this study we focus on the propagation of waves with a finite temporal support and do not consider periodic waves, we require that

$$\frac{\partial u}{\partial \zeta} \Big|_{\zeta \rightarrow \infty} = 0, \quad (\text{S12})$$

from which we obtain $C = 0$. Substitution of Eq. (S11) into Eq. (S9)₂ yields

$$\frac{\partial^2 \theta}{\partial \zeta^2} = C_1 \theta + C_3 \theta^3 \quad (\text{S13})$$

with

$$C_1 = 6\beta K_\theta, \quad \text{and} \quad C_3 = -\frac{2\beta c^2}{c_0^2 - c^2}. \quad (\text{S14})$$

Eq. (S13) is the Klein-Gordon equation with cubic nonlinearities, which admits analytical solution in the form of

$$\theta(x, t) = A \operatorname{sech} \left(\frac{x - ct}{W} \right), \quad (\text{S15})$$

where A , c and W denote the amplitude, speed and width of the pulses. Moreover, by substituting Eq. (S15) into Eq. (S13), the solution for the displacement is found as

$$u(x, t) = \begin{cases} \frac{aA^2 W}{2(1 - c^2/c_0^2)} \left[1 - \tanh \left(\frac{x - ct}{W} \right) \right], & \text{for } c > 0 \\ \frac{aA^2 W}{2(1 - c^2/c_0^2)} \left[-1 - \tanh \left(\frac{x - ct}{W} \right) \right], & \text{for } c < 0 \end{cases} \quad (\text{S16})$$

since for $c > 0$ (i.e. for solitons propagating from left to right) $u(\zeta \rightarrow \infty) = 0$, whereas for $c < 0$ (i.e. for solitons propagating from right to left) $u(\zeta \rightarrow -\infty) = 0$. Eqs (S15)-(S16) reveal an important feature of our system: its ability to support an elastic vector soliton. In fact, in our nonlinear system two components one translational and one rotational are coupled together and co-propagate without distortion nor splitting.

Next, we determine the relation between A , c , W and the geometry of the system. To this end, we substitute the solution (S15) into Eq. (S13) and find that the latter is identically satisfied only if

$$c = \pm c_0 \sqrt{\frac{6K_\theta}{A^2 + 6K_\theta}}, \quad (\text{S17})$$

and

$$W = a \sqrt{\frac{\alpha^2(K_s - K_\theta) - 6K_\theta/(A^2 + 6K_\theta)}{6\alpha^2 K_\theta}}. \quad (\text{S18})$$

Eqs. (S15)-(S16) define the elastic vector solitons that propagate in our system. However, the existence of such waves require that W and c are real numbers. Inspection of Eqs. (S17)

and (S18) reveals that this condition is satisfied only if

$$\mathcal{A}_{\text{upper}} > A > \mathcal{A}_{\text{lower}}, \quad \text{with } \mathcal{A}_{\text{upper}} = -\mathcal{A}_{\text{lower}} = \sqrt{\frac{6K_\theta}{\alpha^2(K_s - K_\theta)} - 6K_\theta}. \quad (\text{S19})$$

Notably, Eq. (S19) defines an amplitude gap for solitons, since it indicates that solitary waves with $A \in [\mathcal{A}_{\text{lower}}, \mathcal{A}_{\text{upper}}]$ cannot propagate in our system. Note that for the specific structure used in this study, $\mathcal{A}_{\text{upper}} = 0.12$ and $\mathcal{A}_{\text{lower}} = -0.12$.

Finally, the displacement and rotation induced by the propagating elastic vector solitons at the i -th pair of crosses can be determined from Eqs. (S15)-(S16) as

$$\theta_i(t) = \theta(x = ia, t) = A \operatorname{sech} \left(\frac{ia - ct}{W} \right), \quad (\text{S20})$$

and

$$u_i(t) = \begin{cases} \frac{aA^2W}{2(1 - c^2/c_0^2)} \left[1 - \tanh \left(\frac{ia - ct}{W} \right) \right], & \text{for } c > 0, \\ \frac{aA^2W}{2(1 - c^2/c_0^2)} \left[-1 - \tanh \left(\frac{ia - ct}{W} \right) \right], & \text{for } c < 0. \end{cases} \quad (\text{S21})$$

Equivalence between Eq. (S13) and the modified Korteweg-de Vries equation At this point we want to emphasize that the modified Korteweg-de Vries (modified KdV) equation can be written into the continuous governing equation of our system (the Klein-Gordon equation with cubic non-linearity given in Eq. (S13)). Here is the general form of the modified KdV equation (3):

$$\frac{\partial \theta}{\partial t} + F_1 \frac{\partial^3 \theta}{\partial x^3} - F_2 \theta^2 \frac{\partial \theta}{\partial x} = 0, \quad (\text{S22})$$

F_1 and F_2 being constants. To demonstrate such equivalence, we first rewrite Eq. (S22) in terms of travelling wave coordinate $\zeta = x - ct$, obtaining

$$-c \frac{\partial \theta}{\partial \zeta} + F_1 \frac{\partial^3 \theta}{\partial \zeta^3} - F_2 \theta^2 \frac{\partial \theta}{\partial \zeta} = 0, \quad (\text{S23})$$

and then integrate Eq. (S23) with respect to ζ yields

$$-c\theta + F_1 \frac{\partial^2 \theta}{\partial \zeta^2} - F_2 \theta^3 = 0, \quad (\text{S24})$$

considering that the integration constant is zero. This last equation can be rewritten in the same form of Eq. (S13) with

$$C_1 = \frac{c}{F_1}, \quad \text{and} \quad C_2 = \frac{F_2}{F_1} \quad (\text{S25})$$

S4 Numerical simulations

Since it is extremely challenging to derive an analytical solution that captures the interaction between the solitons propagating in our system, to study the collisions between the pulses supported by our system we numerically integrate the $2N$ coupled ordinary differential equations given by Eqs. (S3) for a given set of initial and boundary conditions. Specifically, in our simulations we consider 500 pairs of crosses and use $K_s = 0.02$, $K_\theta = 1.5 \times 10^{-4}$ and $\alpha = 1.8$. We use the 4th order Runge-Kutta method (via the Matlab function `ode45`) to numerically solve Eqs. (S3) (the code implemented in MATLAB is available online). As initial conditions we set $u_i = 0$, $\theta_i = 0$, $\dot{u}_i = 0$, $\dot{\theta}_i = 0$ for all pairs of crosses. Moreover, to excite solitons, we simply apply the analytical solution given by Eqs. (S20) and (S21) to the first and last unit of the chain. More specifically, at the left end we impose

$$\begin{aligned} \theta_1(t) &= A_{\text{left}} \operatorname{sech} \left(\frac{-c_{\text{left}}(t - t_0)}{W_{\text{left}}} \right), \\ u_1(t) &= \frac{aA_{\text{left}}^2 W_{\text{left}}}{2(1 - c_{\text{left}}^2/c_0^2)} \left[1 - \tanh \left(\frac{-c_{\text{left}}(t - t_0)}{W_{\text{left}}} \right) \right] \end{aligned} \quad (\text{S26})$$

where W_{left} is given by Eq. (S18) and c_{left} is the positive solution of Eq. (S17). Moreover, t_0 is a parameter introduced to ensure that $\theta_1 \rightarrow 0$ and $u_1 \rightarrow 0$ at $t = 0$ (in all our simulations we use $t_0 = 0.1$ sec). Differently, at the right end (i.e. for $i = N$) we impose

$$\begin{aligned} \theta_N(t) &= A_{\text{right}} \operatorname{sech} \left(\frac{-c_{\text{right}}(t - t_0)}{W_{\text{right}}} \right), \\ u_N(t) &= \frac{aA_{\text{right}}^2 W_{\text{right}}}{2(1 - c_{\text{right}}^2/c_0^2)} \left[-1 - \tanh \left(\frac{-c_{\text{right}}(t - t_0)}{W_{\text{right}}} \right) \right] \end{aligned} \quad (\text{S27})$$

where W_{right} is also determined by Eq. (S18) and c_{left} is the negative solution of Eq. (S17).

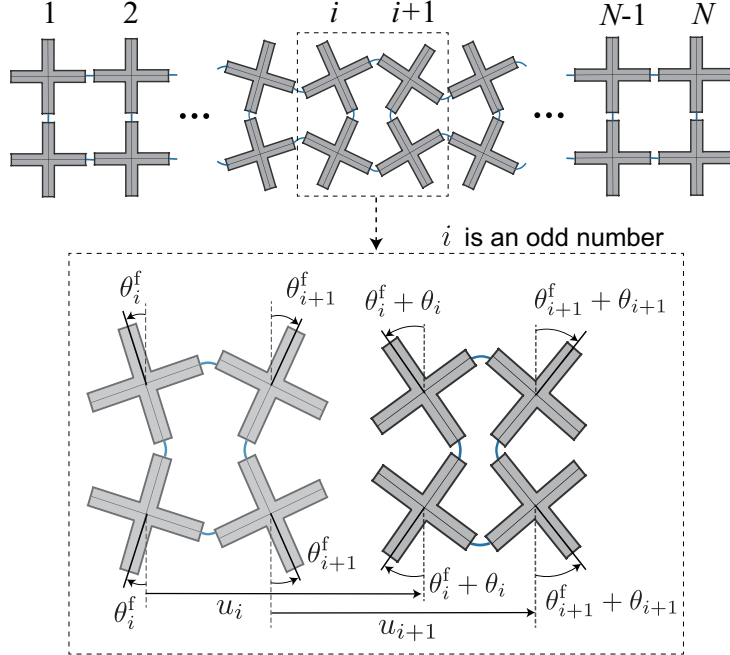


Figure S4: Schematics of the structure considered in this study with a frozen soliton located at its center.

As a part of this study we also consider frozen solitons of different amplitude A_f in the middle of the chain and numerically investigate their effect on the propagation of solitary waves initiated at the left end. In this case the discrete governing equations of the system (Eqs. (S3)) modify to

$$\begin{aligned} \frac{a^2}{c_0^2} \frac{\partial^2 u_i}{\partial t^2} &= u_{i+1} - 2u_i + u_{i-1} - \frac{a}{2 \cos \theta_i^f} [\cos(\theta_{i+1} + \theta_{i+1}^f) - \cos(\theta_{i-1} + \theta_{i-1}^f)], \\ \frac{a^2}{c_0^2 \alpha^2} \frac{\partial^2 \theta_i}{\partial t^2} &= -K_\theta (\theta_{i+1} + 4\theta_i + \theta_{i-1}) + K_s \cos(\theta_i + \theta_i^f) \left[\sin(\theta_{i+1} + \theta_{i+1}^f) \right. \\ &\quad \left. + \sin(\theta_{i-1} + \theta_{i-1}^f) - 2 \sin(\theta_i + \theta_i^f) \right] - \sin(\theta_i + \theta_i^f) \left[2 \cos(\theta_i^f) (u_{i+1} - u_{i-1}) / a \right. \\ &\quad \left. + 4 \cos(\theta_i^f) - \cos(\theta_{i+1} + \theta_{i+1}^f) - 2 \cos(\theta_i + \theta_i^f) - \cos(\theta_{i-1} + \theta_{i-1}^f) \right]. \end{aligned} \quad (S28)$$

where θ_i^f is the initial rotation of the i -th pair of crosses due introduced because of the frozen pulse. For the specific case of a frozen soliton placed in middle of the chain,

$$\theta_i^f = A_f \operatorname{sech} \left[\frac{a(i - N/2)}{W_f} \right], \quad (S29)$$

where A_f denotes the amplitude of frozen soliton and W_f is the width of the frozen soliton, which is determined by Eq. (S18) setting $A = A_f$. As for boundary conditions, we apply input the theoretical solution at the left end as Eqs. (S26) and fixed boundary on the right end, i.e.,

$$\theta_N(t) = 0, \quad u_N(t) = 0 \quad (\text{S30})$$

Finally, we note that the numerical results for pulses characterized by $|A_{\text{left}}| < 0.12$ ($|A_{\text{right}}| < 0.12$) are obtained using Eqs. (S26) (Eqs. (S27)) with $W_{\text{left}} = 1$ ($W_{\text{right}} = 1$). This is because for $|A_{\text{left}}| < 0.12$ ($|A_{\text{right}}| < 0.12$) the width of the pulse given by Eq. (S18) is imaginary. Although this choice of width is arbitrary, quantitatively identical results are obtained for any real width (I).

S5 Additional results

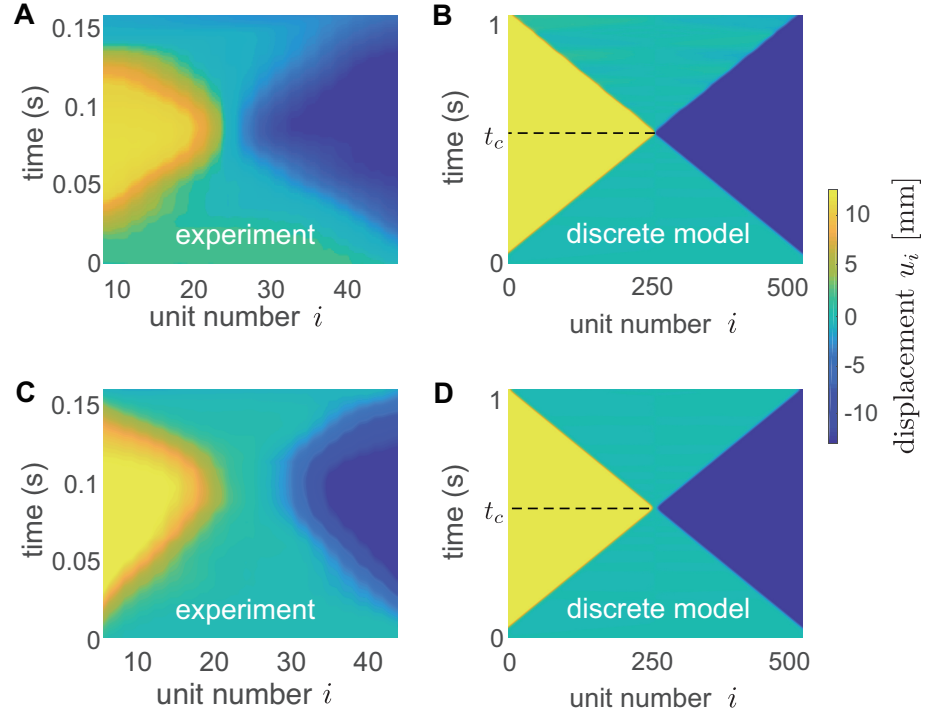


Figure S5: Displacement signal. (A)-(B) Longitudinal displacement of the pairs of crosses during the propagation of the pulses, as recorded in (A) experiments and (B) numerical simulations. The pulses excited at the left and right end are characterized by $A_{\text{left}} = 0.2$ and $A_{\text{right}} = 0.2$, respectively. (C)-(D) Longitudinal displacement of the pairs of crosses during the propagation of the pulses, as recorded in (C) experiments and (D) numerical simulations. The pulses excited at the left and right end are characterized by $A_{\text{left}} = -0.2$ and $A_{\text{right}} = 0.2$, respectively. In (C) and (D) we find that the units near collision point do not move - an indication of anomalous collisional dynamics.

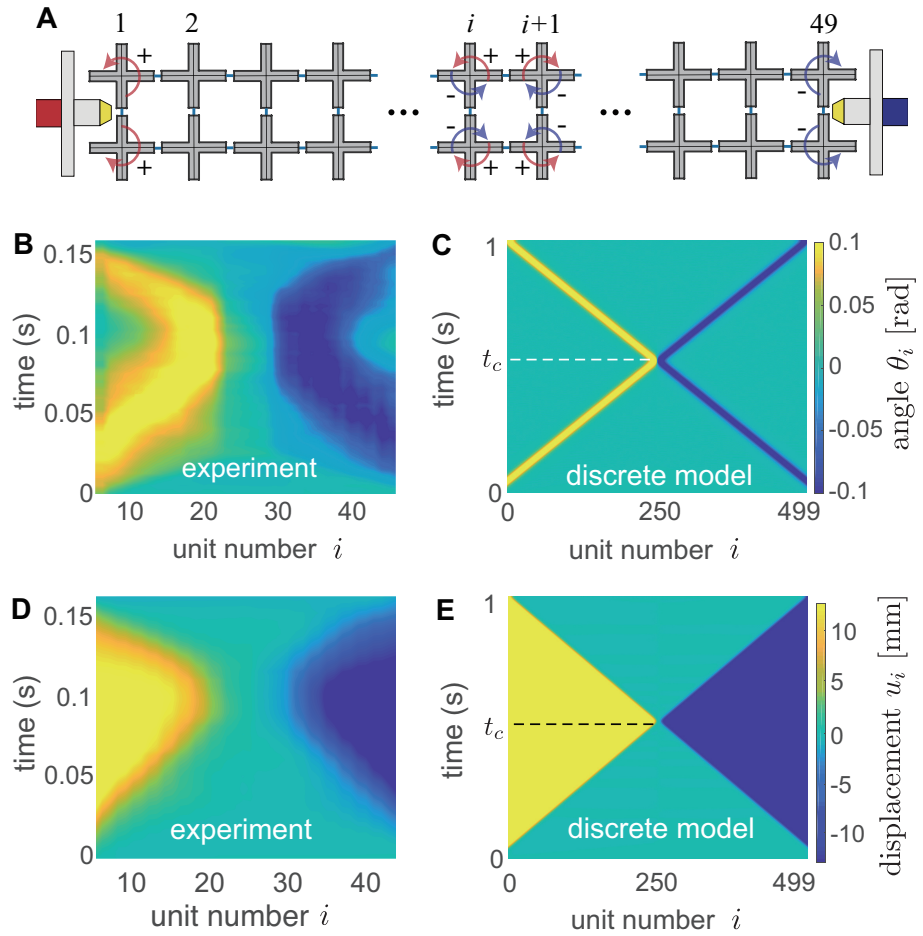


Figure S6: A chain with odd pairs of crosses. (A) We consider a chain with $N = 49$ pair of crosses. To initiate a solution at the right end that induces negative rotations, we use an impactor that hits the mid-point of the last pair. (B)-(C) Rotation of the pairs of crosses during the propagation of the pulses, as recorded in (B) experiments and (C) numerical simulations. (D)-(E) Longitudinal displacement of the pairs of crosses during the propagation of the pulses, as recorded in (D) experiments and (E) numerical simulations. The pulses excited at the left and right end are characterized by $A_{\text{left}} = 0.2$ and $A_{\text{right}} = -0.2$, respectively. The experiments are conducted on a chain with 49 pairs of crosses, whereas in the numerical simulations we consider 499 units.

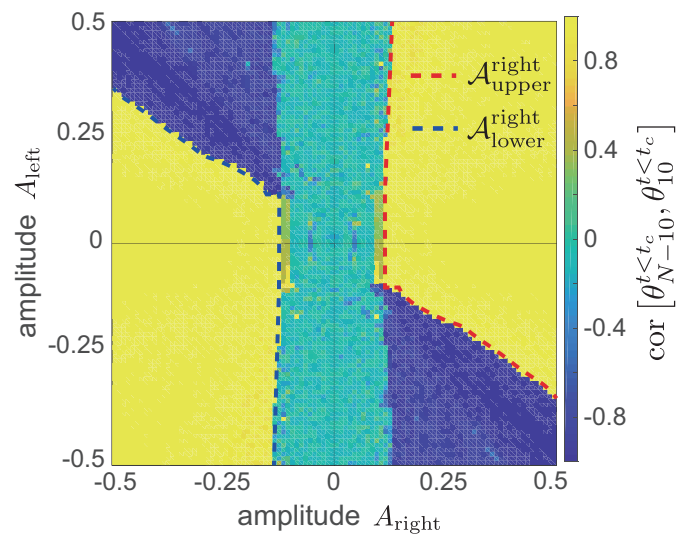


Figure S7: Numerically obtained cross-correlation between $\theta_{10}(t < t_c)$ and $\theta_{N-10}(t > t_c)$ as a function of A_{left} and A_{right} .

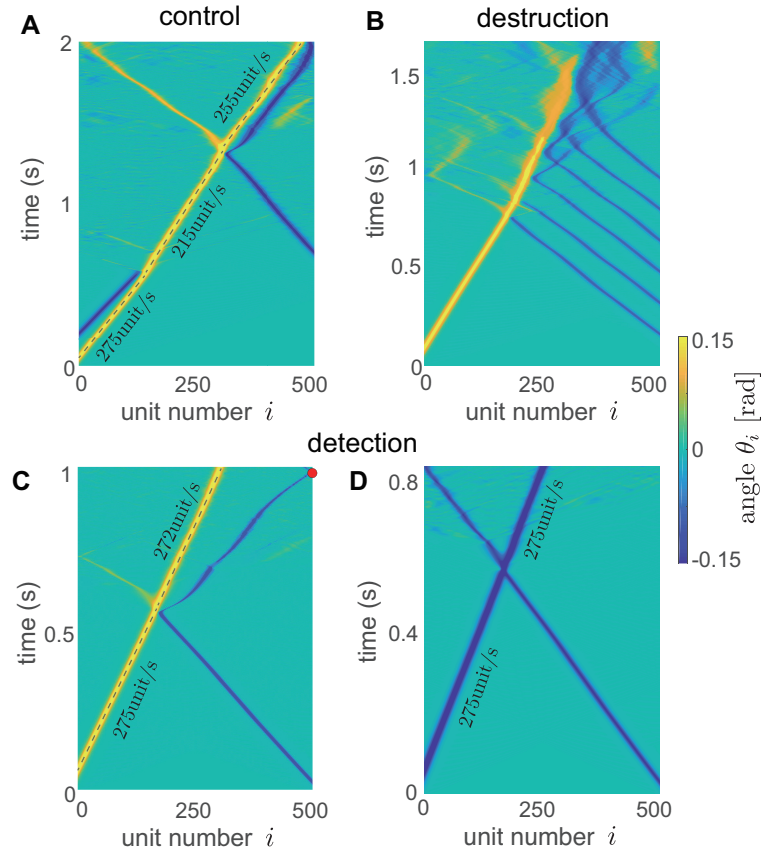


Figure S8: Anomalous collisions can be exploited to actively manipulate and control the propagation of pulses. (A) Anomalous collisions provide opportunities to remotely induce changes in the propagation velocity of a soliton. To demonstrate this, we consider a left-initiated pulse with $A_{\text{left},1} = 0.4$ and $c = 275 \text{ unit/s}$ and use the interactions with a soliton subsequently excited at the left end to reduce its velocity to $c = 215 \text{ unit/s}$ and with a right-initiated solitary wave to then accelerate it to $c = 255 \text{ unit/s}$. (B) Anomalous collision can be exploited to block the propagation of a soliton. Specifically, a large propagating soliton can be blocked by sending a sequence of relatively small pulses with opposite rotation direction. As an example, we consider a left-initiated soliton with $A_{\text{left}} = 0.4$ and six right-initiated solitons with $A_{\text{right},k} = -0.2$ (with $k = 1, \dots, 6$). Each of the six collisions results in energy radiation to linear waves or to other small amplitude solitons and reduces the amplitude of the left-initiated pulse, which eventually vanishes as its amplitude falls within the amplitude gap of the structure. Therefore, six small pulses efficiently mitigate and destroy the main left-initiated soliton at $t = 2\text{s}$. (C)-(D) Anomalous collisions can also be exploited to probe the direction of the rotational component of a pulse. To demonstrate this, we consider a main left-initiated soliton with $A_{\text{left}} = \pm 0.4$ and a probing, small right-initiated pulse with $A_{\text{right}} = -0.18$. If $A_{\text{left}} = 0.4$ (C), the "echo" of the probing soliton reaches the right end before the main soliton, indicating that it has been reflected by the main soliton. From this information, we therefore deduce that the main soliton is of positive amplitude. If $A_{\text{left}} = -0.4$ (D), no "echo" is observed, as the probe penetrate the main soliton. From this information, we therefore deduce that the main soliton is of negative amplitude. Finally, it is important to point out that, since the probing soliton carries much less energy than the main one, the latter is almost unaltered by the collision (i.e. its velocity changes from 275unit/s to 272unit/s).

References

1. B. Deng, P. Wang, Q. He, V. Tournat, K. Bertoldi, *Nature Communications* **9**, 3410 (2018).
2. M. Senn, <https://www.mathworks.com/matlabcentral/fileexchange/50994-digital-image-correlation-and-tracking> (2016).
3. A. Polyanin, V. Zaitsev, *Handbook of Nonlinear Partial Differential Equations, Second Edition* (Chapman and Hall/CRC, 2011).